Available online at www.sciencedirect.com

ScienceDirect

Proceedings of the Combustion Institute 38 (2021) 1685–1693

Proceedings of the Combustion Institute

www.elsevier.com/locate/proci

Exploiting line-mixing effects for laser absorption spectroscopy at extreme combustion pressures

Daniel D. Lee [a,b,*], Fabio A. Bendana [a], Anil P. Nair [a], Stephen A. Danczyk [b], William A. Hargus Jr. [b], R. Mitchell Spearrin [a]

[a] *Department of Mechanical and Aerospace Engineering, University of California, Los Angeles (UCLA), Los Angeles, CA 90095, USA*

[b] *U.S. Air Force Research Laboratory, Edwards Air Force Base, CA 93524, USA*

Received 7 November 2019; accepted 5 August 2020
Available online 19 October 2020

Abstract

A unique spectroscopic strategy has been developed for laser absorption sensing of carbon monoxide (CO) and carbon dioxide (CO_2) at extreme pressures ($P > 50$ atm) relevant to modern combustion devices. The strategy exploits the band narrowing effects of line mixing, which acutely impact spectrally dense regions, such as bandheads, where line spacing is small. Line mixing is shown to counter collisional line-broadening effects that reduce differential absorption at elevated pressures and often limit the pressure range of laser absorption methods. In this work, the R-branch bandheads of CO and CO_2, which are only observed at high temperatures relevant to combustion, are targeted near 2.3 μm and 4.2 μm, respectively. Spectral line-mixing models were developed for each bandhead region to account for the collision-induced population transfer rates between rotational energy states over a wide range of elevated temperatures and pressures. Modified-exponential-gap models using the relaxation matrix formalism were shown to capture the thermodynamic dependence of the population transfer rates and enabled scaling. Differential absorption at the bandheads was observed to increase by up to a factor of ten at high gas densities, due to line-mixing effects, enabling detection with relatively narrow-band tunable semi-conductor lasers. With refined spectroscopic models, laser absorption measurements of temperature, CO, and CO_2 were demonstrated over a range of high pressures (up to 104 atm) in a sub-scale rocket combustor operated with kerosene and supercritical methane.

Keywords: Absorption spectroscopy; High pressure combustion; Line mixing; Rocket propulsion

1. Introduction

Combustion at extreme pressures (> 50 atm) is of increasing significance as engine developers push the limits of power density, efficiency, and emissions suppression. Several ultra-clean piston-engine concepts are designed to operate at peak

* Corresponding author at: Department of Mechanical and Aerospace Engineering, University of California, Los Angeles (UCLA), Los Angeles, CA 90095, USA.
E-mail address: daniellee9101@ucla.edu (D.D. Lee).

https://doi.org/10.1016/j.proci.2020.08.037
1540-7489

pressures in excess of 100 atm [1], while modern liquid-propellant rockets may have steady-state combustion chamber pressures above 200 atm. At these very high pressures, many of the underlying assumptions present in combustion modeling become less reliable and predictive capability for engineering design requires new understanding. To elucidate combustion physics at high-pressure conditions, controlled experiments coupled with comprehensive diagnostics are needed. Unfortunately, most state-of-the-art combustion diagnostics have been limited to much lower pressures ($<$ 20 atm), prompting the need to develop new high-pressure diagnostic techniques suitable for interrogating the next generation of combustion systems.

Laser absorption spectroscopy (LAS) has been extensively utilized for non-intrusive in situ measurements of temperature and species in harsh combustion environments [2]. For small molecules (n $<$ 5 atoms) at moderate pressures ($<$ 10 atm), LAS techniques commonly target individual spectral lines or transitions, which can be resolved with narrow-band lasers and interpreted with a few spectroscopic parameters. However, at higher pressures, this line-specific analytical approach falters, largely due to collisional line broadening, which scales linearly with pressure. Collisional broadening leads to a blending of adjacent spectral lines that: (1) decreases differential absorption (i.e. difference in peak-to-valley absorption in a local spectral domain), (2) causes cross-species interference, and (3) complicates spectral modeling and interpretation. For LAS methods with limited spectral bandwidth, the reduction in differential absorption leads to an effective pressure limit in harsh environments, where non-absorption losses are typical and difficult to distinguish from molecular absorption without spectral structure.

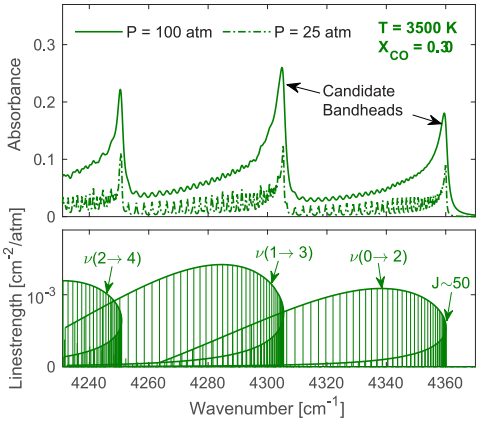

Fig. 1. Simulated CO absorbance and linestrengths near 2.3 μm (excluding line-mixing effects) at representative high-temperature combustion conditions using the HITEMP spectral database [3].

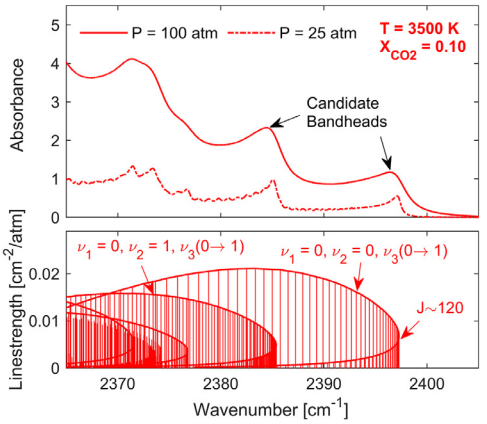

Fig. 2. Simulated CO_2 absorbance and linestrengths near 4.2 μm (excluding line-mixing effects) at representative high-temperature combustion conditions using the HITEMP spectral database [3].

While few quantitative species diagnostics have been demonstrated above 20 atm in practical combustion environments, some successes can be noted. Caswell et al. developed near-infrared sources with a wide spectral range to measure methane, water vapor, and temperature up to 30 atm in a gas turbine combustor [4]. Mattison et al. similarly probed the near-infrared water spectrum to achieve in-cylinder measurements up to 54 atm in a HCCI piston-engine [5]. In the mid-wave infrared, Goldenstein [6] and Spearrin et al. [7] performed LAS of H_2O and CO in a pulse detonation combustor (PDC) at pressures up to 50 atm, targeting the fundamental vibrational bands. More recently, we extended CO sensing to 70 atm in a rocket combustor using a similar mid-infrared approach [8]. For CO_2, LAS near 20 atm was performed in an entrained-flow coal gasifier, targeting the CO_2 spectra near 2.0 μm [9]. Themes of these prior works include leveraging advancements in more broadly tunable sources and carefully selecting molecules and spectral lines that have intrinsically low broadening.

This paper describes a new approach to high-pressure laser absorption sensing that exploits the vibrational band narrowing effects of line mixing to significantly extend pressure capability. Line mixing relates to collision-induced changes in rotational energy that result in transfers of absorption intensity from weak to strong regions within a vibrational band. Line-mixing effects are pronounced in spectrally dense regions, where line spacing is small, such as bandheads. For CO and CO_2, the R-branch bandheads near 2.3 μm and 4.2 μm, respectively, become active at combustion temperatures, as shown in Figs. 1 and 2. While collisional line broadening diminishes the differential absorption of specific rovibrational transitions, line

mixing counters this effect by narrowing and amplifying bandheads, which are comprised of many closely spaced lines. Here, we target the aforementioned bandheads for laser absorption sensing, investigate and characterize line-mixing effects on the local spectra over a range of high-pressure and high-temperature conditions, and demonstrate the pressure-capability of the method via quantitative species measurements in a sub-scale rocket combustor at pressures up to 104 atm.

2. Spectroscopic approach

2.1. Line-mixing theory

Spectral line mixing is often observed at high gas densities, where collision-induced changes in rotational energy distort the molecular spectra within a vibrational band. Generally, these collisional effects favor intensity exchanges from weak to strong absorption regions, resulting in a vibrational band narrowing effect and promoting larger differential absorption. This phenomenon is more prominent in spectrally dense regions where line spacing is small, such as bandheads, which are shown in the linestrength plots of Figs. 1 and 2. A spectral bandhead is the result of vibrational and rotational energy coupling that yields decreasing line spacing in the R-branches of CO and CO_2 stretch bands. For these particular bands, the convergence and wrap-around of spectral lines is only observed at high temperatures, where high rotational energy states are populated. Figures 1 and 2 illustrate the set of transitions that make up several CO and CO_2 bandheads near 2.3 μm and 4.2 μm, respectively. As discussed, line mixing is expected to amplify the bandhead peak intensity and enhance differential absorption at elevated pressures, rendering these features strategic candidates for LAS sensing in extreme combustion environments.

To model absorption and account for line-mixing effects, we implement a relaxation matrix formalism [10] to represent the state-to-state population transfer rates. A more rigorous theoretical discussion with modeling process details can be found in other papers from our research group [11,12]; the steps are truncated here for brevity. For a monochromatic light source at frequency ν [cm^{-1}], the spectral absorbance, α_ν, through a gas medium can be described by the transmitted and incident light intensities, I_t and I_0, respectively, via the Beer-Lambert law. Absorbance can then be related to thermophysical flow properties using the following relationship:

$$\alpha_\nu = -\ln\left(\frac{I_t}{I_0}\right)_\nu = \frac{nL}{\pi}\,\mathrm{Im}(\mathbf{d}\cdot\mathbf{G}^{-1}\cdot\boldsymbol{\rho}\cdot\mathbf{d}) \tag{1}$$

where n [molec · cm^{-3}] is the total number density of the absorbing species, L [cm] is the optical path length, $\boldsymbol{\rho}$ is a diagonal matrix containing the lower state Boltzmann population fractions, and $\mathbf{d}$ [cm^{-1}/(molec · cm^{-2})]$^{\frac{1}{2}}$ is a vector of transition amplitudes [13]. $\mathbf{G}$ is a complex matrix given as:

$$G = \nu\mathbf{I} - \boldsymbol{\nu}^0 - iP\mathbf{W} \tag{2}$$

$\mathbf{I}$ represents the identity matrix, $\boldsymbol{\nu}^0$ [cm^{-1}] is a diagonal matrix containing transition frequencies, P [atm] is pressure, and $\mathbf{W}$ [cm^{-1}/atm] is the relaxation matrix.

The relaxation matrix, $\mathbf{W}$, contains all collisional influences on the spectral shape [14]. The real diagonal terms of $\mathbf{W}$ consist of the broadening coefficients, γ_J [cm^{-1}/atm], and the imaginary diagonal terms are the pressure shift coefficients, $\Delta\nu_J^0$ [cm^{-1}/atm]. The real off-diagonal terms are proportional to the state-to-state population transfer rates, $R_{J\to K}$ [cm^{-1}/atm], from initial rotational energy level J to the final rotational energy level K and the imaginary off-diagonal components of $\mathbf{W}$ describe contributions from rovibrational dephasing [15]. It is important to note that broadening coefficients can be expressed in terms of the state-to-state population transfer rates (R) that describe line-mixing effects [16]:

$$\gamma_J = \frac{1}{2}\left[\sum_{J''\neq K''} R_{J''\to K''} + \sum_{J'\neq K'} R_{J'\to K'}\right] \tag{3}$$

Here, prime ($'$) and double prime ($''$) refer to the upper and lower states.

In this work, the real off-diagonal elements of $\mathbf{W}$ were modeled using the following modified-exponential-gap (MEG) law [17,18]:

$$W_{JK} = a_1(T)\left[\frac{1+a_4\left(\frac{E_J''}{a_2 k_B T}\right)}{1+a_4\left(\frac{E_J''}{k_B T}\right)}\right]^2 \times \exp\left[\frac{-a_3\left(E_K'' - E_J''\right)}{k_B T}\right] \tag{4}$$

Here, E'' [cm^{-1}] is the lower state energy of the transition and a_i are empirical MEG law coefficients. Methods for obtaining these coefficients are briefly discussed in Section 2.2, with more detailed discussions in [11,12]. It is important to note that the temperature dependence of the real off-diagonal components is captured through $a_1(T)$, which follows the power law, analogous to broadening coefficient. To fully complete the relaxation matrix, the upward and downward population transfer rates are related through the detailed-balance principle [19]:

$$\rho_J R_{J\to K} = \rho_K R_{K\to J} \tag{5}$$

This indicates that line mixing induces a vibrational band narrowing effect by favoring population transfers from weak transitions to strong transitions, supporting physical observations of the spectral structure.

Notably, when multiple collision partners are present, the full relaxation matrix can be expressed as a mixture-weighted summation of the individual perturber contributions:

$$\mathbf{W} = \sum_{B} X_B \mathbf{W}_{A-B} \tag{6}$$

With **W** fully defined, the simulated spectra, incorporating line-mixing effects, can now be scaled over a range of temperatures and pressures.

2.2. Spectral modeling

To characterize line-mixing effects in the CO and CO_2 bandheads, high-temperature and high-pressure experiments were conducted utilizing a high-enthalpy shock tube facility at UCLA. Scanned-wavelength direct absorption measurements of CO near 2.3 μm were obtained at pressures and temperatures ranging from 5–25 atm and 2000–4000 K, respectively, using pure CO gas. CO_2 measurements near 4.2 μm were conducted at pressures ranging from 20–60 atm and a slightly lower temperature range of 2000–3000 K, to minimize dissociation. Shock tube experiments for CO_2 were carried out in an argon (Ar) bath gas to minimize non-ideal gas dynamics (e.g. boundary layers) and provide greater experimental control over thermodynamic conditions.

In order to describe collision-induced population transfer rates, the modified-exponential gap law given in Eq. (4) was incorporated into the absorbance modeling framework. Species-specific MEG law coefficients, a_i, were obtained by least-squares fitting the high-pressure absorbance data from the shock tube facility with the absorbance model, given by Eq. (1). This procedure was carried out for both CO and CO_2 over the range of thermodynamic conditions aforementioned to capture the temperature and pressure dependence of the relaxation matrix. The measured species-specific MEG law coefficients can be found in Table 1, while the collisional broadening coefficients can be found in separate works [11,12]. It should be noted that collisional broadening and line mixing contributions are separated in the relaxation matrix formalism. To obtain collisional broadening coefficients and their respective temperature dependencies, shock tube experiments were conducted at low pressures (< 2.5 atm), where individual spectral transitions

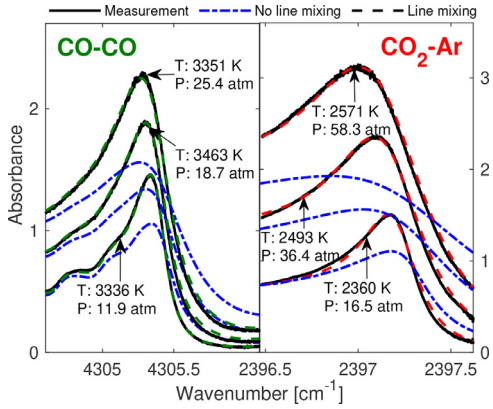

Fig. 3. Measured spectral absorbance for (*left*) CO-CO and (*right*) CO_2-Ar compared to the developed MEG model used to capture line-mixing effects over a range of pressures.

are distinct and contributions due to line mixing are negligible. These broadening coefficients are then implemented in the absorbance modeling framework to study line-mixing at higher-pressures, wherein the off-diagonal elements of the relaxation matrix, related to mixing rates, can be determined. Figure 3 highlights the pressure scalability of the updated absorbance model accounting for line-mixing effects. Notably, the line-mixing model exhibits excellent agreement with the measured CO and CO_2 spectra over a range of pressures. Additionally, Fig. 3 illustrates that without line mixing, the simulated spectra poorly represents the measured absorbance near the bandhead, where most of the population transfers occur. The simulated spectra with no line-mixing effects was modeled as a sum of Voigt profiles using the HITEMP spectral database [3] with updated self-broadening coefficients for CO [11] and Ar-broadening coefficients for CO_2 [12].

In order to extend the spectral line mixing models for CO and CO_2 developed in the shock tube to rocket combustion environments, additional assumptions are required to account for the dependence of the relaxation matrix on mixture composition. Namely, this involves scaling arguments that relate collisional line broadening coefficients and the population transfer rates for various per-

Table 1
MEG law parameters used in this work.

	a_1 [10^{-3} $cm^{-1}atm^{-1}$]	a_2	a_3	a_4
CO-CO	1.52 ± 0.16[a]	0.51 ± 0.05	5.21 ± 0.10	2
CO_2-Ar	53.94 ± 2.49[b]	4.98 ± 0.25	3.19 ± 0.13	2

[a] T_{ref} = 1500 K with power-law exponent of 1.28 ± 0.06 [11]
[b] T_{ref} = 1200 K with power-law exponent of 2.06 ± 0.07 [12]

turbing species. Species-specific broadening coefficients, which are assigned to the real diagonal components of the relaxation matrices, are found in the literature for H_2O, CO_2, CO, and O_2 perturbers [20,21]. This accounts for $>$ 80% of a typical rocket combustion gas mixture, the remainder of which is assumed to be N_2. The population transfer rates, related to the real off-diagonal elements of the species-specific relaxation matrices, are obtained by scaling the measured rates (CO-CO and CO_2-Ar) by the ratio of broadening coefficients for each perturber (H_2O, CO_2, CO, O_2), as shown in Eqs. (7) and (8). The basis for this assumption is the sum rule (Eq. (3)) that indicates that broadening coefficients scale similarly to the population transfer rates.

$$\mathbf{W}_{\mathrm{CO}-mix} = \sum_B X_B \mathbf{W}_{\mathrm{CO}-\mathrm{CO}} \left(\frac{\gamma_{\mathrm{CO}-B}}{\gamma_{\mathrm{CO}-\mathrm{CO}}} \right) \tag{7}$$

$$\mathbf{W}_{\mathrm{CO_2}-mix} = \sum_B X_B \mathbf{W}_{\mathrm{CO_2}-\mathrm{Ar}} \left(\frac{\gamma_{\mathrm{CO_2}-B}}{\gamma_{\mathrm{CO_2}-\mathrm{Ar}}} \right) \tag{8}$$

Recall the collisional broadening coefficients and population transfer rates that comprise $\mathbf{W}_{\mathrm{CO}-\mathrm{CO}}$ and $\mathbf{W}_{\mathrm{CO_2}-\mathrm{Ar}}$ have been measured experimentally [11,12]. For the sensing application discussed herein, chemical equilibrium is assumed to dictate mixture composition at a given operating condition for the purposes of weighting broadening coefficients and mixing parameters in Eqs. (7) and (8). These modeling adjustments provide a basis for high-pressure spectral interpretation of LAS measurements in various combustion environments.

3. Sensor design

3.1. Optical interface

Figure 4 illustrates a simplified optomechanical configuration representing the hardware interface for LAS on the target sub-scale liquid-propellant rocket combustor. For brevity, a thorough description of the experimental setup can be found in additional works by the authors [8,22]; however, details pertaining to the line-mixing sensing strategy are discussed herein. To target the CO and CO_2 bandheads, a distributed-feedback (DFB) diode laser with $\sim$10 mW output power was centered near 2322 nm and an interband cascade laser (ICL) with $\sim$5 mW output power was centered near 4173 nm, respectively. For two-color thermometry measurements, an additional DFB quantum cascade laser (QCL) with $\sim$50 mW output power is employed to probe the fundamental CO absorption band near 4979 nm [8,22].

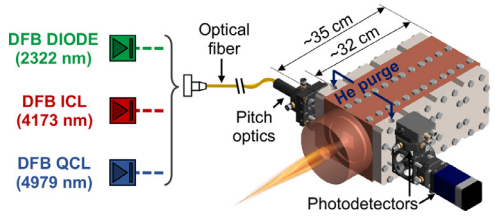

Fig. 4. Optical interface with rocket combustor, including a graphical depiction of remote-light delivery and collection optics, for high-pressure CO and CO_2 measurements.

An inherent challenge presented by this approach is the wavelength-specific nature of many optical components (e.g. detectors, fibers) that potentially increases sensor complexity to pitch and collect multiplexed light at very different wavelengths. To reconcile this, the incident light is combined and focused into a hollow-core fiber with broad transmissivity for remote light delivery [23,24]. The fiber output is then re-collimated and transmitted across the combustion chamber through two wedged sapphire windows over a 2.5 cm transverse optical path length. A beam splitter is installed to separate the transmitted light so that each beam can be spectrally filtered for its respective wavelength before being collected on separate thermoelectrically-cooled photodetectors. An InGaAs photodetector (Thorlabs PDA10D) with a 15 MHz bandwidth is utilized for 2.3 μm light and a MCT photovoltaic detector (Vigo PVI-4TE-5-1) with a 10 MHz bandwidth is utilized for 4.2 μm and 5.0 μm light.

Measurements were conducted $\sim$32 cm downstream of the single-element-injector, where complete combustion/mixing is most likely to occur. Raw detector data were collected at a sample rate of 10 MHz for 5-s intervals with hot-fires spanning 2–3 s in duration. Due to hardware limitations, experiments were limited to two light sources per test. Therefore, hot-fires were conducted twice for each condition, alternating between the ICL targeting the CO_2 bandhead and the QCL targeting the CO fundamental band. The steady-state pressure trace and laser absorption signals for subsequent hot-fire tests targeting the same condition typically agreed within 2%, or within measurement uncertainty, suggesting reasonable repeatability of experiments.

3.2. Laser tuning parameters

Scanned-wavelength modulation spectroscopy with second harmonic ($2f$) normalized detection was implemented for all rocket combustor measurements in order to minimize dynamic non-absorption-related light intensity distortion. The $1f$ normalized-WMS-$2f$, with background subtraction, provides a well-established technique to extract signals strongly related to differential absorption while rejecting noise associated with beam steering, scattering, and thermal emission [25]. Measurements are conducted by superimpos-

Table 2
Laser scan and modulation parameters.

ν [nm]	a_s [cm^{-1}]	f_s [Hz]	a_m [cm^{-1}]	f_m [kHz]
2322	2.55	100	0.48	50
4173	0.63	100	0.36	20
4979	0.13	100	0.50	20

ing a fast sine-wave modulation on a slow sine-wave scan from which the harmonic components are extracted using digital lock-in amplification and frequency filtering. Within the framework of scanned-WMS, the scan depth, a_s, modulation depth, a_m, and associated frequencies, f_s and f_m, can be adjusted to optimize signal quality. Additionally, the center wavelength of each laser was slightly adjusted ($<$ 0.07 nm) across different combustor conditions to account for pressure shift in the spectra and maximize the WMS signal. The parameters for each laser are listed in Table 2 and were selected as a compromise between WMS-2f signal quality (SNR) and effective measurement rate. Further details on the parametric optimization strategy can be found in [8,22].

In probing high-pressure spectra, rapidly tunable distributed feedback lasers are often unable to resolve differential absorption within achievable modulation depths due to collisional broadening and blending of adjacent features. Consequently, a common desire is to increase spectral bandwidth with broadband sources. In this work, the band narrowing effects of line mixing are shown, via spectral simulation, to increase differential absorption by up to a factor of ten within the narrow tuning range of the selected sources, suggesting persistently strong harmonic signals with increasing pressure at the somewhat modest scan and modulation depths shown in Table 2. To prove capability, experiments were performed in a high-pressure combustor.

4. Experimental results

4.1. Thermochemistry measurements

A series of field measurements were conducted over a range of pressures and propellant mixture ratios (MR) from 25–104 atm and 2.2–4.6, respectively, on a single-element-injector rocket combustor with CH_4/GOx and RP-2/GOx propellant combinations. The test facility is located at the Air Force Research Laboratory on Edwards Air Force Base, CA USA. Figure 5 shows a representative hot-fire test including time-resolved measurements of pressure and the corresponding WMS-2f/1f signals at 4.2 μm, 2.3 μm, and 5.0 μm for a steady-state chamber condition of 27.4 atm and MR of 2.33. An abrupt increase in all WMS-2f/1f signals

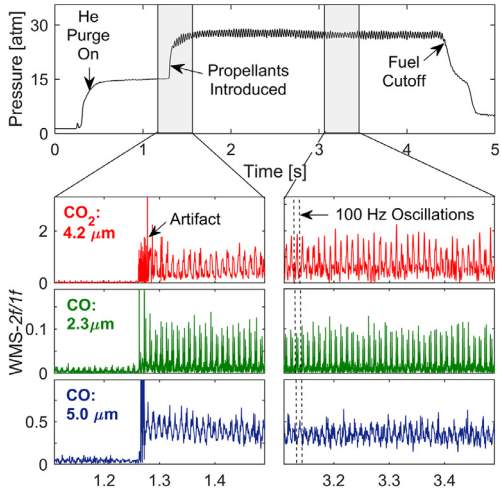

Fig. 5. Time evolution of chamber pressure for a representative test and the corresponding WMS-2f/1f signals (background subtracted) for CO_2 near 4.2 μm and CO near 2.3 μm and 5.0 μm.

was observed around 1.3 s, corresponding to the introduction of propellants and ignition.

For all three wavelengths, the raw optical signal was averaged over the steady-state region to improve signal-to-noise ratio (SNR) and was processed through a digital lock-in amplifier to extract the WMS harmonics, from which species and temperature can be inferred. Figures 6 and 7 compare the measured WMS-2f/1f signals targeting the CO and CO_2 bandheads, respectively, to simulated WMS-2f/1f signals with and without the updated line-mixing model discussed in Section 2.2. Notably, the CO measurements exhibit favorable SNR

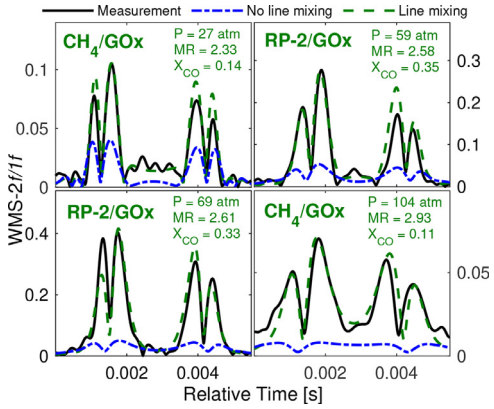

Fig. 6. Measured WMS-2f/1f signals targeting CO compared to simulated WMS-2f/1f signals with and without the updated line-mixing model over a range of mixture ratios and pressures.

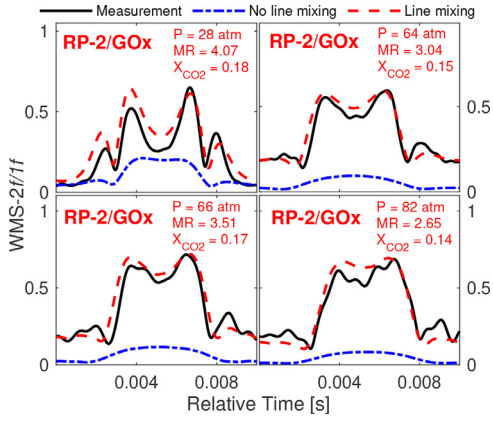

Fig. 7. Measured WMS-2*f*/1*f* signals targeting CO_2 compared to simulated WMS-2*f*/1*f* signals with and without the updated line-mixing model over a range of mixture ratios and pressures.

at pressures up to 104 atm and the CO_2 measurements exhibit similar signal quality up to 82 atm, the highest respective pressures tested for either sensor. Notably, the divergence between the models with and without line-mixing effects increases with pressure.

The best-fit WMS signals using the refined spectral model were used to quantitatively infer mole fraction and temperature. The ratio of peak WMS signals from 2.3 μm and 5.0 μm was utilized to first obtain temperature, which was then used to infer CO and CO_2 concentration based on absolute signal magnitude [8,26]. Figure 8 compares the measured temperatures and mole fractions to chemical equilibrium solver (NASA CEA) predictions [27] for RP-2/GOx, which can be used to assess combustion progress. The chemical equilibrium results are bound by the highest and lowest pressures measured, respectively. In order to obtain mole fraction measurements above 70 atm, where the SNR of the CO fundamental band measurements was deemed too low, CEA temperature was assumed. The inferred temperatures from all tests followed the expected trends, but were slightly lower (generally by 100–300 K) than equilibrium temperature, typical of incomplete combustion, poor mixing, heat losses, or a cold boundary layer. Temperature and multi-species measurements can be used to evaluate overall combustor performance/efficiency and anchor to computational models that inform engine design.

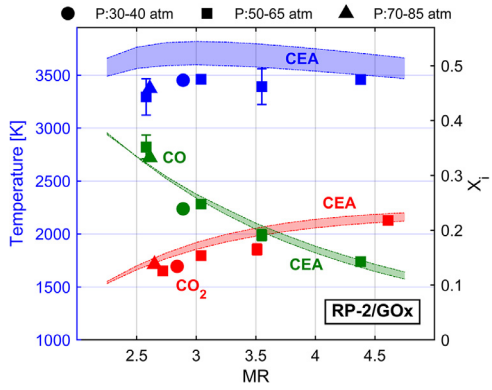

Fig. 8. Temperature and species measurements with representative error bars at steady-state combustor conditions compared to NASA CEA predictions over a range of mixture ratios and pressures for kerosene and oxygen.

4.2. Measurement uncertainty

In this paper, we follow the Taylor series method (TSM) of uncertainty propagation [28]. The main factors considered in calculating the uncertainties in the measured temperatures and mole fractions include: (1) uncertainty in pressure measurements, (2) uncertainty in the spectroscopic model related to composition-dependent collisional broadening and mixture ratio (MR), and (3) mechanical noise induced from the harsh combustion environment. For the uncertainty in mole fraction, the temperature uncertainty has been considered in addition to the aforementioned contributors since concentration inference requires a temperature input. The total temperature uncertainty was estimated to be 8–11% for all experiments and both CO and CO_2 mole fraction uncertainties were approximately 10–13%, with the largest uncertainty corresponding to the highest pressure. In order to improve these values for future studies, refinement of the spectroscopic models and further noise mitigation is necessary. Despite this, the mole fraction measurements are consistent with total carbon conservation and both temperature and species trend with the anticipated values from chemical equilibrium over the range of mixture ratios tested. More details regarding uncertainty analysis can be found in Appendix A.

5. Conclusion

A novel laser absorption sensing strategy was developed for quantitative measurements of CO and CO_2 at high combustion pressures (P > 50 atm). The technique exploits the vibrational band narrowing effects of line mixing, which acutely amplify differential absorption at bandheads, and counter the effects of collisional line broadening. In this work, the CO and CO_2 R-branch bandheads near 2.3 μm and 4.2 μm, respectively, are strategically targeted to extend the pressure-range capability of in situ sensing of gas properties in combustion environments using relatively narrowband light sources. Field measurements were con-

ducted over a range of high pressures in a subscale rocket combustor operated with kerosene and supercritical methane. In order to quantitatively interpret the measured WMS-2*f*/1*f* signals, spectral line-mixing models were developed for each bandhead utilizing a high-enthalpy shock tube facility. The refined spectroscopic models employ a modified-exponential gap law to thermodynamically scale line-mixing effects, which enabled quantitative inference of temperature, CO, and CO_2 in the liquid-propellant rocket combustor. To the authors' knowledge this work represents significant extensions in demonstrated pressure capability, to 104 atm and 82 atm, respectively, for in situ CO and CO_2 species measurements in practical combustion devices. More importantly, the enhanced pressure capability enabled by the novel spectroscopic strategy provides for a valuable new tool to experimentally investigate and engineer the next generation of high-pressure combustion systems.

Declaration of Competing Interest

None.

Acknowledgments

This work was primarily sponsored by the Air Force Research Laboratory under Award No. 16-EPA-RQ-09. The authors would like to thank Dr. John W. Bennewitz for help in setting up the data acquisition system, and Dr. Daniel I. Pineda and Dr. Chuyu Wei for ongoing support in developing the line-mixing model. The fundamental spectroscopy work is supported by the US National Science Foundation, Award No. 1752516.

Appendix A. Uncertainty analysis

The uncertainty analysis presented here largely follows that of Nair et al. [29]. The uncertainties in temperature and mole fraction of species A were calculated using Eqs. A.1 and A.2, which account for the uncertainty factors described in Section 4.2.

$$(\Delta T)^2 = (\Delta T_{\Delta P})^2 + (\Delta T_{\text{Spec.}})^2 + (\Delta T_{\text{SNR}})^2 \quad \text{(A.1)}$$

$$(\Delta X_A)^2 = (\Delta X_{A,\Delta P})^2 + (\Delta X_{A,\text{Spec.}})^2 + (\Delta X_{A,\text{SNR}})^2 + (\Delta X_{\text{A},\Delta T})^2 \quad \text{(A.2)}$$

Figure A.1 presents the visual summary of the uncertainties for each variable along with contributions from the various dependent variables. Typically, the uncertainties in the spectroscopic model

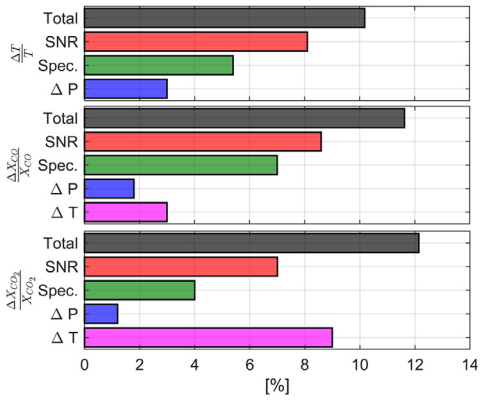

Fig. A.1. Representative uncertainties for temperature, T, CO mole fraction, X_{CO}, and CO_2 mole fraction, X_{CO_2}, for a hot-fire test at P = 56 atm and MR = 3.5

and the environmental noise were the largest contributors. Mole fraction of CO_2 was most susceptible to the temperature uncertainty. The pressure uncertainty was taken from the difference between the measured pressure variations and the mean pressure during the test. The inverse of the SNR from each test was used to estimate uncertainty due to mechanical noise. In order to estimate the spectroscopic model uncertainty, we define a mixture-weighted broadening coefficient, $\gamma_{\text{A-mix}}(T)$, as:

$$\gamma_{A-\text{mix}}(T) = \sum_B X_B(\gamma_{A-B}(T)) \quad \text{(A.3)}$$

Per Eqs. (7) and (8), the uncertainty in the spectroscopic model strongly depends on the uncertainty in the scaling factor, which is the ratio between $\gamma_{A-\text{mix}}(T)$ and broadening coefficients, $\gamma_{\text{CO-CO}}$ and $\gamma_{\text{CO}_2-\text{Ar}}$. The uncertainty of the mixture-weighted broadening coefficient, $\Delta\gamma_{A-\text{mix}}(T)$, is attributed to the uncertainty in the broadening coefficients of individual perturbers, $\Delta\gamma_{A-B}(T)$, and the uncertainty in local equivalence ratio, $\Delta\phi$, (which determines composition) as shown in Eq. (A.4).

$$(\Delta\gamma_{A-\text{mix}}(T))^2 = \sum_B [(\gamma_{A-B}(T)\Delta X_B)^2 + (X_B\Delta\gamma_{A-B}(T))^2] \quad \text{(A.4)}$$

The mole fractions of the collision partners, X_B, were calculated from NASA CEA [27] and the uncertainty, ΔX_B, was estimated based on the uncertainty in local equivalence ratio:

$$(\Delta X_B)^2 = \left(\frac{\partial X_B}{\partial\phi}\Delta\phi\right)^2 \quad \text{(A.5)}$$

The uncertainty in the temperature-dependent collisional broadening coefficient, $\Delta\gamma_{A-B}(T)$, for species A with collision partner B is calculated as

follows:

$$\left(\frac{\Delta\gamma_{A-B}(T)}{\gamma_{A-B}(T)}\right)^2 = \left(\frac{\Delta\gamma_{A-B}(T_0)}{\gamma_{A-B}(T_0)}\right)^2 + N_{B^2}\left(\frac{\Delta T}{T}\right)^2 + \left[\ln\left(\frac{T_0}{T}\right)\Delta N_B\right]^2 \quad (A.6)$$

The uncertainties in collisional broadening coefficient, $\Delta\gamma_{A-B}$, at reference temperature, T_0, and temperature-dependent exponent, ΔN_B, were taken from literature [11,20,21]. The uncertainties in γ_{CO-CO} and γ_{CO_2-Ar} were determined from prior works by the authors [11,12].

References

[1] R.D. Reitz, G. Duraisamy, *Progress Energy Combust. Sci.* 46 (2015) 12–71, doi:10.1016/j.pecs.2014.05.003.

[2] C.S. Goldenstein, R.M. Spearrin, J.B. Jeffries, R.K. Hanson, *Progress Energy Combust. Sci.* 60 (2017) 132–176, doi:10.1016/j.pecs.2016.12.002.

[3] L. Rothman, I. Gordon, R. Barber, H. Dothe, R. Gamache, A. Goldman, V. Perevalov, S. Tashkun, J. Tennyson, *J. Quant. Spectrosc. Radiat. Transf.* 111 (15) (2010) 2139–2150, doi:10.1016/j.jqsrt.2010.05.001.

[4] A.W. Caswell, T. Kraetschmer, K. Rein, S.T. Sanders, S. Roy, D.T. Shouse, J.R. Gord, *Appl. Opt.* 49 (26) (2010) 4963, doi:10.1364/AO.49.004963.

[5] D. Mattison, J. Jeffries, R. Hanson, R. Steeper, S. De Zilwa, J. Dec, M. Sjoberg, W. Hwang, *Proc. Combust. Inst.* 31 (1) (2007) 791–798, doi:10.1016/j.proci.2006.07.048.

[6] C.S. Goldenstein, R.M. Spearrin, J.B. Jeffries, R.K. Hanson, *Proc. Combust. Inst.* 35 (3) (2015) 3739–3747, doi:10.1016/j.proci.2014.05.027.

[7] R.M. Spearrin, C.S. Goldenstein, J.B. Jeffries, R.K. Hanson, *Appl. Opt.* 53 (9) (2014) 1938–1946, doi:10.1364/AO.53.001938.

[8] D.D. Lee, F.A. Bendana, S.A. Schumaker, R.M. Spearrin, *Appl. Phys. B: Lasers Opt.* 124 (5) (2018) 77, doi:10.1007/s00340-018-6945-6.

[9] K. Sun, R. Sur, X. Chao, J.B. Jeffries, R.K. Hanson, R.J. Pummill, K.J. Whitty, *Proc. Combust. Inst.* 34 (2) (2013) 3593–3601, doi:10.1016/j.proci.2012.05.018.

[10] U. Fano, *Phys. Rev.* 131 (1) (1963) 259–268, doi:10.1103/PhysRev.131.259.

[11] F.A. Bendana, D.D. Lee, C. Wei, D.I. Pineda, R.M. Spearrin, *J. Quant. Spectrosc. Radiat. Transf.* 239 (2019) 106636, doi:10.1016/j.jqsrt.2019.106636.

[12] D.D. Lee, F.A. Bendana, A.P. Nair, D.I. Pineda, R.M. Spearrin, *J. Quant. Spectrosc. Radiat. Transf.* (2020) 107135, doi:10.1016/j.jqsrt.2020.107135.

[13] L.L. Strow, D. Reuter, *Appl. Opt.* 27 (5) (1988) 872, doi:10.1364/AO.27.000872.

[14] D. Romanini, K.K. Lehmann, *J. Chem. Phys.* 105 (1) (1996) 81–88, doi:10.1063/1.471883.

[15] R.G. Gordon, *J. Chem. Phys.* 45 (5) (1966) 1649–1655, doi:10.1063/1.1727808.

[16] J.M. Hartmann, C. Boulet, D. Robert, *Collisional Effects on Molecular Spectra*, Elsevier, 2008, doi:10.1016/B978-0-444-52017-3.X0001-5.

[17] M.L. Koszykowski, L.A. Rahn, R.E. Palmer, M.E. Coltrin, *J. Phys. Chem.* 91 (1) (1987) 41–46, doi:10.1021/j100285a012.

[18] L. Rahn, R. Palmer, M. Koszykowski, D. Greenhalgh, *Chem. Phys. Lett.* 133 (6) (1987) 513–516, doi:10.1016/0009-2614(87)80069-6.

[19] A. Ben-Reuven, *Phys. Rev.* 145 (1) (1966) 7–22, doi:10.1103/PhysRev.145.7.

[20] J.M. Hartmann, L. Rosenmann, M.Y. Perrin, J. Taine, *Appl. Opt.* 27 (15) (1988) 3063, doi:10.1364/ao.27.003063.

[21] L. Rosenmann, J.M. Hartmann, M.Y. Perrin, J. Taine, *Appl. Opt.* 27 (18) (1988) 3902, doi:10.1364/AO.27.003902.

[22] F.A. Bendana, D.D. Lee, S.A. Schumaker, S.A. Danczyk, R.M. Spearrin, *Appl. Phys. B* 125 (11) (2019) 204, doi:10.1007/s00340-019-7320-y.

[23] J.M. Kriesel, N. Gat, B.E. Bernacki, R.L. Erikson, B.D. Cannon, T.L. Myers, C.M. Bledt, J.A. Harrington, in: Proceedings of SPIE - The International Society for Optical Engineering, 8018, 2011, p. 80180V, doi:10.1117/12.882840.

[24] R.M. Spearrin, C.S. Goldenstein, I.A. Schultz, J.B. Jeffries, R.K. Hanson, *Appl. Phys. B* 117 (2) (2014) 689–698, doi:10.1007/s00340-014-5884-0.

[25] G.B. Rieker, J.B. Jeffries, R.K. Hanson, *Appl. Opt.* 48 (29) (2009) 5546–5560, doi:10.1364/AO.48.005546.

[26] K. Sun, X. Chao, R. Sur, C.S. Goldenstein, J.B. Jeffries, R.K. Hanson, *Measur. Sci. Technol.* 24 (12) (2013) 125203, doi:10.1088/0957-0233/24/12/125203.

[27] B.J. McBride, S. Gordon, *Computer Program for Calculation of Complex Chemical Equilibrium Compositions and Applications*, NASA, 1996. January

[28] H.W. Coleman, W.G. Steele, *Experimentation, Validation, and Uncertainty Analysis for Engineers*, 3rd, John Wiley & Sons, Inc., Hoboken, NJ, USA, 2009.

[29] A.P. Nair, D.D. Lee, D.I. Pineda, J. Kriesel, W.A.H. Jr, J.W. Bennewitz, S.A. Danczyk, R.M. Spearrin, *Appl. Phys. B* 126 (8) (2020) 138, doi:10.1007/s00340-020-07483-8.